

Semi-Implicit Eulerian Version of Nonhydrostatic HIRLAM

Rein Rõõm
Tartu Observatory
room aai.ee

Aarne Männik
Tartu University
aarne aai.ee

1 Introduction

Semi-implicit (SI) integration is employed in majority of forecast models, because it reduces the phase speeds of fast acoustical and buoyancy waves, and, as a result, provides larger numerical stability and time-step.

In the case of the non-hydrostatic (NH) HIRLAM, the acoustical mode is filtered prior to the discretization, making use of the physical approximation of the acoustic wave speed $c_a \rightarrow \infty$ (which is the essence of the anelastic approximation in pressure coordinates). Thus, subject to the modification are the fast buoyancy waves with propagation speed $c_b \approx 100\text{m/s}$.

In following, a short description of the SINH scheme for HIRLAM is presented. In general, the SINH model keeps to the ideology of SI Eulerian scheme of hydrostatic (HS) HIRLAM. However, a lot of modifications are needed due to the adjusted surface pressure approximation.

2 Basic formalism

Prognostic equations of the SINH HIRLAM are (like in the explicit case), equations for the horizontal momentum and temperature

$$\frac{\partial \mathbf{v}}{\partial t} = -\hat{\mathbf{G}}(\phi + \frac{1}{2}\overline{\Delta_{tt}\varphi}^\eta) + \mathbf{F}_v, \quad \frac{\partial T}{\partial t} = S\frac{1}{2}\overline{\Delta_{tt}\omega}^\eta + F_T. \quad (1)$$

Notation is that as used in the *Manual* (Källén, 1996) and in the explicit NH HIRLAM (Rõõm 2001, Männik and Rõõm 2001). $\hat{\mathbf{G}}$ is the isobaric horizontal gradient in hybrid coordinates, ϕ and φ are the baric and thermic geopotentials, $\Delta_{tt}f \equiv f^{t-\Delta t} + f^{t+\Delta t} - 2f^t$ is the second order time difference,

$$S_k = \left(\frac{\varkappa\alpha T - \overline{\Delta_\eta T}^\eta}{\Delta_\eta p} \right)_k$$

presents the stability (or stratification) parameter on level k , and \mathbf{F}_v , F_T are the explicit hydrostatic tendencies of \mathbf{v} and T , respectively, on the time level t . Combining the barometric formula and the ω -tendency equation (not presented

here, look in (Männik and Rõõm, 2001)) with the temperature equation, the following relationships can be proved for the second order differences of φ and ω :

$$\frac{1}{2}\overline{\Delta_{tt}\varphi}^\eta = -\Delta t^2 \sum_{k'=k}^{Nlev} (N^2 \Delta_\eta \phi)_{k'+1/2} + \mu_\varphi, \quad \frac{1}{2}\overline{\Delta_{tt}\omega}^\eta = -\Delta t \left(\frac{p}{H^\eta} \right)^2 \delta_p \phi + \overline{\mu_\omega}^\eta. \quad (2)$$

Here H and N are the scale-height and Väisälä frequency:

$$H = RT/g, \quad N_{k+1/2}^2 = \left[\frac{\overline{\alpha R S^\eta} p^2}{(H^\eta)^2 \Delta_\eta p^\eta} \right]_{k+1/2},$$

δ_p is the vertical pressure-gradient in hybrid-coordinate representation, and

$$(\mu_\varphi)_k = \sum_{k'=k+1}^{Nlev} [\alpha R (\mu_T + \Delta t S \overline{\mu_\omega}^\eta)]'_k + \frac{1}{2} [\alpha R (\mu_T + \Delta t S \overline{\mu_\omega}^\eta)]_k.$$

Variables μ_T and μ_ω are specified via definition

$$\mu_X \equiv \Delta t F_X - X^t + X^{t-\Delta t},$$

and $\alpha_k = \ln p_{k+1/2} - \ln p_{k-1/2}$.

Thus, the second order differences (2) are dependent, beside of known functions μ_φ and μ_ω (both determined by meteorological fields on the time levels t and $t - \Delta t$), also on the baric geopotential ϕ on the time level t . Consequently, the tendency equations (1) can be integrated after the baric geopotential ϕ is specified.

2.1 Equation for the baric geopotential

The equation for baric geopotential can be derived, differentiating the anelastic pressure-space continuity equation

$$\hat{\mathbf{G}}^+ \cdot \mathbf{v} + \delta_p^+ \omega = 0$$

(where $\hat{\mathbf{G}}^+$ and δ_p^+ are the horizontal and vertical pressure-coordinate divergence operators in hybrid coordinates) in time and using the tendency equations for \mathbf{v} and ω :

$$\hat{\mathbf{G}}^+ \cdot \hat{\mathbf{G}} \phi + \delta_p^+ \left(\frac{p^2}{(H^\eta)^2} \delta_p \phi \right) + \hat{\mathbf{G}}^+ \cdot \hat{\mathbf{G}} \left(\frac{1}{2} \overline{\Delta_{tt}\varphi}^\eta \right) = A_\phi,$$

where the source function is

$$A_\phi = \hat{\mathbf{G}}^+ \cdot \mathbf{F}_v + \delta_p^+ F_\omega = 0.$$

The last term on the left side in this equation, with $\Delta_{tt}\varphi$ defined in (2), represents a small perturbing contribution to the explicit baric geopotential equation. It is justified and reasonable to simplify this term, approximating N in (2) with its mean value:

$$N \approx \bar{N}, \quad (3)$$

which yields

$$\frac{1}{2}\Delta_{tt}\bar{\varphi}^\eta = -\Delta t^2\bar{N}^2(\phi_{Nlev} - \phi_k) + \mu_\varphi.$$

As the result, the equation for ϕ becomes

$$(1 + \Delta t^2\bar{N}^2)\hat{\mathbf{G}}^+ \cdot \hat{\mathbf{G}}\phi + \delta_p^+ \left(\frac{p^2}{(\bar{H}^\eta)^2} \delta_p\phi \right) = \hat{\mathbf{G}}^+ \cdot \hat{\mathbf{G}}(\Delta t^2\bar{N}^2\phi_{Nlev} - \mu_\varphi) + A_\phi. \quad (4)$$

This is the basic equation for the baric geopotential in the SI case. It represents a straightforward generalization of the explicit scheme equation, and it transforms to the latter in the limit $\Delta t \rightarrow 0$. Also, the boundary conditions remain the same. As a result, the solution algorithm for (3) is basically the same as in the explicit case.

2.2 On the approximation of the Väisälä frequency

Approximation (3) can be justified only by positive experimental results. Actually, N is changing in broad scale, as demonstrated in Fig. 1. In some sub-domain, N can become even imaginary (i.e., N^2 can become negative).

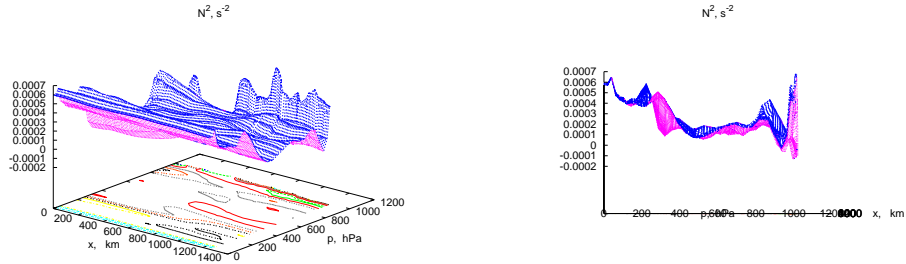


Fig. 1. The vertical cross section of N^2 in plane $x - p$ for the domain and period, presented in Figs. 2 and 3. Left panel - perspective view; right panel - side view in the x -direction.

As the numerical experimentation shows, in practice it is advantageous to take \bar{N} moderately exceeding the domain-averaged value $\langle N \rangle$:

$$\bar{N} = 1.5\langle N \rangle \div 2.0\langle N \rangle, \quad \langle N \rangle = \frac{1}{NlonNlatNlev} \sum_{ijk} N_{ijk}. \quad (5)$$

This approximation increases the stability of the SI scheme and allows for larger time steps.

It should be pointed, that approximation of the implicit terms in the elliptic equation is not novel. Analogous approximation is applied in the SI hydrostatic Eulerian version of HIRLAM, where the reference temperature $T_r = 300$ K and reference surface pressure $p_r = 800$ hPa are used to stabilize the semi-implicit Poisson solver. The method goes back to the pioneering works on the SI approach (Simmons et al. 1978, Côté et al. 1983).

3 Numerical implementation

The described algorithm is implemented as an extension to the existing experimental version of the explicit-Eulerian NH HIRLAM (Männik and Rõõm, 2001). Some examples of modeling with the new scheme are presented in Figs. 2 (surface pressure) and 3 (vertical cross-sections of wind and temperature fields). Presented is the 24h forecast on the 0.1 degree resolution, 114X100 point, 31 level grid.

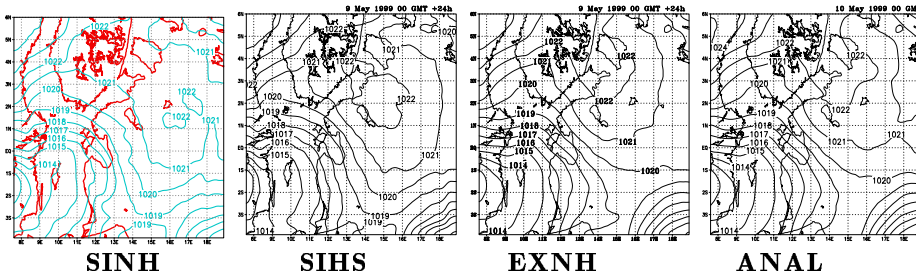


Fig. 2. 24h MSL pressure forecast with the semi-implicit non-hydrostatic, semi-implicit hydrostatic, and explicit non-hydrostatic schemes, compared to the analysis for the same time.

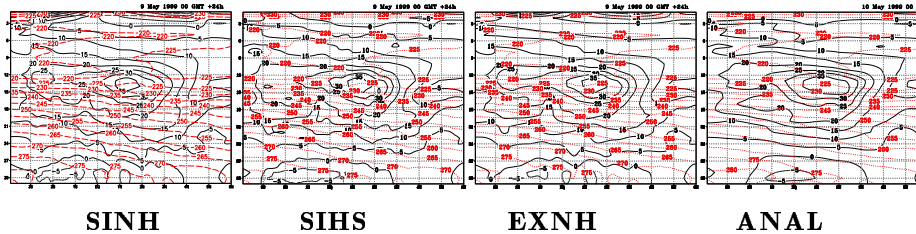


Fig. 3. 24h forecast for the vertical cross-sections ($\lambda = 14E$) of U -wind and temperature with the semi-implicit non-hydrostatic, semi-implicit hydrostatic, and explicit non-hydrostatic schemes, compared to the analysis for the same time.

The figures demonstrate reasonable quality and close coincidence of the new algorithm with other schemes (SIHS and explicit NH). Still, more close is the SINH forecast to the results of its hydrostatic relative, SIHS scheme. Both they lose to the explicit scheme, when compared with the analysis. Of course, this is

just a single experiment, and it is premature to make far-reaching conclusions from the single run. It demonstrates, however, that the SINH-scheme does work. The effective mean buoyancy frequency (5) in this experiment is chosen $\overline{N} = 1.5(N)$. The time step is 120 s (explicit scheme enables 60 s time-step in this experiment). As the numerical experimentation exhibits, the semi-implicit scheme is stable up to $\Delta t \approx \Delta x/U$. Examples of top time-steps for different resolutions and maximum wind-speeds are presented in Table 1.

TABLE 1

Δx	U	$\Delta x/U$	Explicit NH Euler	SINH Euler
11 km	60 m/s	183	60	150
11 km	30 m/s	366	60	300
2 km	20 m/s	100	40	80

The time-consumption rate (computation time per on time step) of the SI model is slightly lower than in the explicit case. The integration algorithm in both schemes is basically the same, and this explains similar time consumption rate. The slight additional economy in the SINH is achieved due to the smaller (in average over many time-steps) number of iterations at solution of the elliptic equation (4), which, in its turn, is determined by the smoothing effect of the SI scheme (which is rather analogous to the smoothing effect of spectral diffusion).

3.1 Problems

In the SINH scheme, the spuriously reflected buoyancy waves may arrive at the top. Reflections are observed at simulations of ideal uniform flows in conditions of the homogeneous stratification, $N = \overline{N} = \text{constant}$, over isolated mountains. In such ideal experiments, the orographically forced waves reach upper boundary $p = 0$, and perform (in the SINH scheme) reflection patterns near the top (Fig. 4). Fortunately, these reflections are trapped near the upper boundary and do not tend to spread over the whole atmosphere. Unfortunately, they could not be absorbed by any sponge layer, as the sponging makes the reflection even stronger. This effect is not observed in the real experiments. The probable explanation is, that in the real conditions the atmosphere is both vertically and horizontally rather non-homogeneous, and the waves are reflected and scattered at the lower levels (mainly at the lower and upper boundaries of the tropopause), long before they reach the top.

4 Conclusions

A semi-implicit Eulerian scheme for non-hydrostatic HIRLAM with the adjusted surface pressure is developed. The new scheme represents a straightforward

generalization of the explicit-Eulerian nonhydrostatic model. Compared to the explicit-Eulerian non-hydrostatic scheme, new model is in medium 2 – 3 times more economical by time consumption.

However, problems are encountered at the top, where spurious, quasi-trapped buoyancy waves can develop. This shortcoming is not crucial, but lowers the model quality, and it should be eliminated in future.

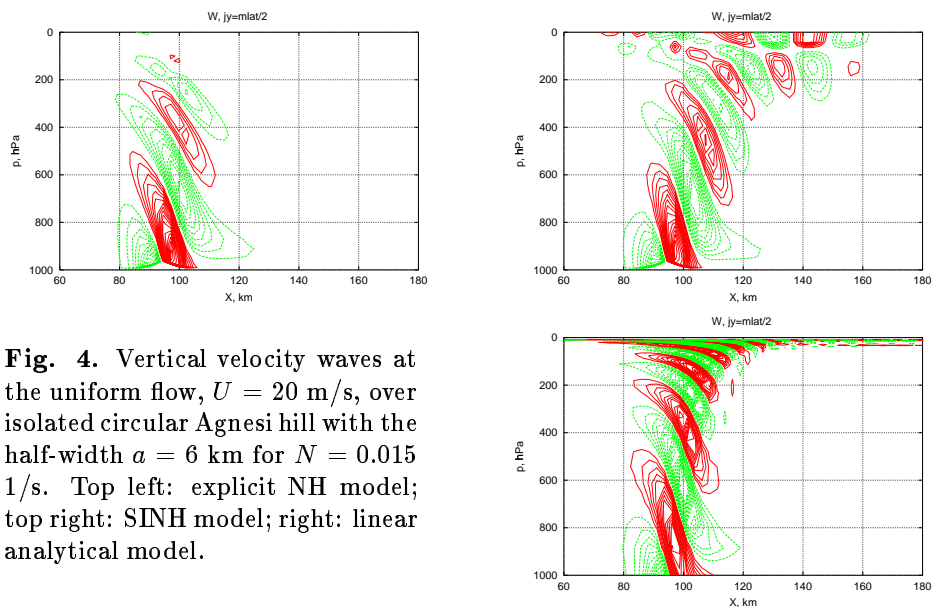


Fig. 4. Vertical velocity waves at the uniform flow, $U = 20$ m/s, over isolated circular Agnesi hill with the half-width $a = 6$ km for $N = 0.015$ 1/s. Top left: explicit NH model; top right: SINH model; right: linear analytical model.

References

- Källén, E., (Editor), 1996: HIRLAM Documentation Manual. SMHI, Norrköping.
- Côté, J., Béland, M., Staniforth, A., 1983: Stability of vertical discretization schemes for semi-implicit primitive equation models: Theory and applications. *Mon. Weather Rev.*, **111**, 1189 - 1207.
- Männik, A., Rõõm, R., 2001: Nonhydrostatic adiabatic kernel for HIRLAM. Part II. Anelastic, hybrid-coordinate, explicit-Eulerian model. *HIRLAM Technical Report, No 49*, SMHI, Norrköping, 55 p.
- Rõõm, R., 2001: Nonhydrostatic adiabatic kernel for HIRLAM. Part I. Fundamentals of nonhydrostatic dynamics in pressure-related coordinates. *HIRLAM Technical Report, No 48*, SMHI, Norrköping, 25 p.
- Simmons, A. J., Hoskins, B. J., Burridge, D. M., 1978: Stability of the semi-implicit method of time integration. *Mon. Weather Rev.*, **106**, 405 - 412.